Inwardly Rotating Spirals in a Nonoscillatory Medium

Harunori N. Yoshikawa[*] and Christian Mathis

Université Côte d'Azur, CNRS, UMR 7351, Laboratoire J.-A. Dieudonné, 06108 Nice Cedex 02, France

Shu Satoh and Yuji Tasaka

Faculty of Engineering, Hokkaido University, N13W8, Sapporo 060-8628, Japan

We report the spontaneous formation of spiral patterns observed at a downward-facing free surface of a horizontal liquid film. The surface is unstable to the Rayleigh-Taylor instability and the resulting liquid discharge from the film can occur in the form of propagating liquid curtains. They are born at the film circular periphery and exhibit patterns of inwardly rotating spiral arms. With the help of a phenomenologically constructed cellular automaton, we show that the patterns arise from the phase locking leading to periodic liquid discharge at constant flow rate over the whole film surface.

The formation of patterns in nonequilibrium systems has attracted much interest in a variety of scientific fields, as understanding self-organization processes provides rich insights into their complex behavior [1]. Spiral patterns emerging through chiral symmetry breaking are of particular interest. The formation has been investigated intensively for waves in excitable media, e.g., in Belousov-Zhabotinsky chemical reaction systems [2]. The behavior of these reaction-diffusion systems is modeled either by coupled differential equations or by cellular automata for excitation and recovery processes [3,4]. Spiral patterns in forced dissipative systems have also been studied. Bodenschatz *et al.* [5] observed patterns of stable spirals and of chaotic spiral defects in a Rayleigh-Bénard convection of a non-Boussinesq fluid. Numerical simulations of the generalized Swift-Hohenberg model reproduce the observed patterns [6]. A theoretical analysis [7] by a phase diffusion equation, which is applicable to a wide variety of nonequilibrium systems [1], shows that the frustration of the local wave number vector drives the motion of convection rolls to produce spiral patterns. The patterns observed in these systems consist of single or multiple curved arms rotating around a core. The rotation occurs with their arms trailing the direction of rotation so that the advancing front of each arm moves outward from the core. Nevertheless, the phase diffusion equation allows spirals propagating both inward and outward [7]. Vanag and Epstein, indeed, discovered inwardly rotating spiral arms in the Belousov-Zhabotinsky reaction in a water-in-oil microemulsion [8]. The observed pattern is called *antispiral*. The formation of antispirals is reproduced by numerical simulations in excitable and oscillatory media [9].

In the present Letter, we report our observation of antispirals at the downward-facing free surface of a liquid film, to which liquid is supplied continuously. The destabilization of the film by the Rayleigh-Taylor (RT) instability leads to liquid discharge from the film in different modes, drops, columns, and curtains, depending on the rate of liquid supply. The RT instability of a film under continuous liquid supply and the dynamics of resulting patterns have been investigated, in particular, for the column mode of discharge [10–15]. We explore the discharge in curtain mode, where spiral patterns are observed, with varying the film lateral extension, the liquid viscosity, and the rate of liquid supply.

The experimental setup is the same as in previous work [13]. A liquid film forms under a grid plate. A given amount
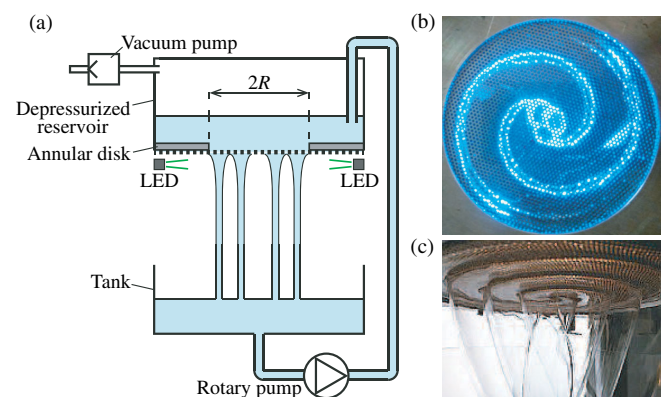

FIG. 1. Experimental setup. (a) Schematic illustration of the whole setup. Holes of the grid plate have a diameter $a = 1$ mm and distributed on a hexagonal lattice with an interhole distance $d = 2$ mm. Uniform liquid supply is assured by a static liquid layer maintained in a depressurized reservoir above the plate. An annular light-emitting diode (LED) lighting system allows us to detect sharp deflections of the free surface by optical observation in top view. (b) A snapshot of a pattern of two spiral curtains in top view. (c) A snapshot of a pattern of single spiral curtain in side view (see Movie 1 in Supplemental Material [16]).
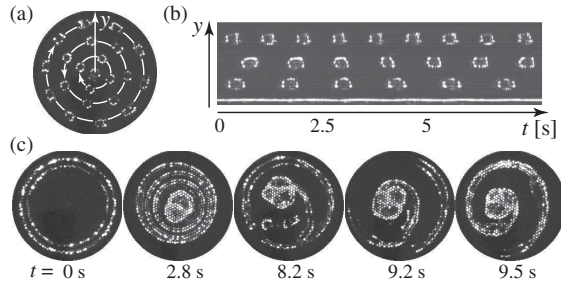
FIG. 2. Some rotating patterns. (a) A snapshot in top view of liquid columns revolving around the center ($R = 45$ mm, $U = 3.8$ mm/s). (b) A space-time diagram constructed from line images along the y axis shown in (a). (c) Formation process of a single armed spiral pattern ($R = 40$ mm, $U = 4.6$ mm/s). The liquid viscosity is 321 mm^2/s for all the results. See Movies 2 and 3 in Supplemental Material [16].

FIG. 3. Spiral patterns formed with a central mask. (a) The number of observed spiral arms m. (b)–(e) Different patterns of different m. The liquid kinematic viscosity ν, the film radius R, and the rate of liquid supply U are (b),(c) 321 mm^2/s, 65 mm, 4.65 mm/s and (d),(e) 197 mm^2/s, 55 mm, 7.12 mm/s. See Movie 4 in Supplemental Material [16].

of liquid U, per unit time and per unit area, is supplied to the film uniformly through holes of the plate (Fig. 1). The lateral extension of the film is varied by masking a peripheral zone of the plate with different annular disks of different inner radii R ($40 \leq R \leq 65$ mm). Three silicone oils of different kinematic viscosities $\nu(= 105, 197, 325$ mm^2/s) are adopted as test liquid. The density and surface tension of these oils are $\rho = 980$ kg/m^3 and $\gamma = 21$ mN/m, respectively. The corresponding capillary length is $l = (\gamma/\rho g)^{1/2} = 1.48$ mm, where g is the gravitational acceleration.

Different modes of discharge are observed with increasing the rate of liquid supply U *or* the Froude number Fr $= U/\sqrt{gl}$ [13]. Rotating patterns form spontaneously when $0.03 \lesssim$ Fr $\lesssim 0.07$. At the smallest limit of this Fr range, the discharge can occur in the form of columns revolving around the center [Fig. 2(a)]. The pattern is not in solid body rotation, as the angular velocity of revolution is smaller for inner columns [Fig. 2(b)]. A slight increase of Fr leads to liquid discharge in curtain mode where spiral patterns in solid body rotation can be observed. A typical formation of spiral curtains starts from the film periphery, where axisymmetric curtains fall periodically. The curtains propagate inward, exhibiting a *target* pattern [Fig. 2(c), $t = 0, 2.8$ s]. The target pattern is not stable: axisymmetric curtains shrink to the center and collapse to form a "core," below which agglomerated conical bubbles are often observed. Curtains then start winding up around the core [Fig. 2(c), $t = 8.2$–9.5 s] and the core shifts to the center of the film. Finally, spiral curtains in steady rotation are established [Figs. 1(b) and 1(c)]. Once formed, the pattern is robust and persists for a long time unless strong perturbations are introduced. To accelerate the formation of spiral curtains, one can mask the central zone of the grid plate, e.g., by placing a cylindrical rod on the plate, as we did with one of a radius $R_0 = 11$ mm for most of the measurements. This artificial defect promotes a quick formation of a spiral core at the center.
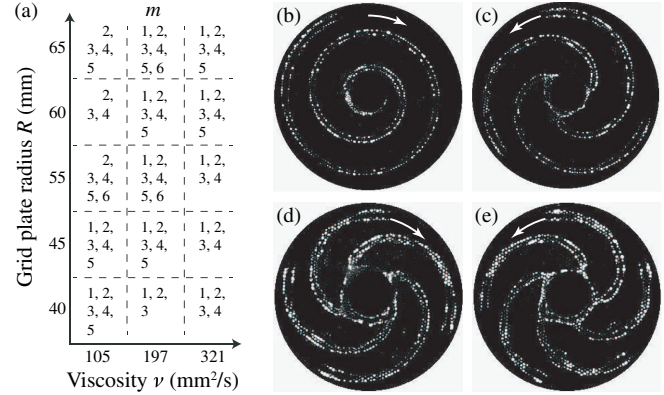
The system in the spiral regime exhibits multistability. Patterns of different numbers m of spiral arms, ranging from 1 to 6, are observed at the same set of values of the control parameters (ν, R, U) [Fig. 3(a)]. In the experiment, no external perturbation was introduced to promote particular patterns: the selection of patterns seems to result from an uncontrollable initial condition. The sense of pattern rotation is also decided randomly: clockwise and counterclockwise rotations are observed with the same probability. The curtains propagate, however, always from the film periphery to the center, leading to the formation of antispirals [Figs. 3(b)–3(e)]. The inward propagation could be explained by the inward capillary force exerted by the curtains on their roots, as the Laplace pressure inclines curtains from the vertical to their concave side [Fig. 1(c)] [17]. The angular speed Ω of the solid body rotation of a pattern is inversely proportional to the number of arms for a given liquid and for a given flow condition [Fig. 4(a)], implying that the frequency $\omega = m\Omega$ of liquid discharge is
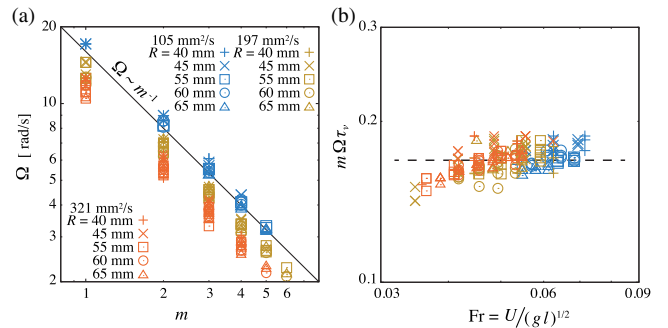

FIG. 4. Temporal characteristics of spiral patterns. (a) The frequency Ω of the solid body rotation of patterns. (b) The frequency of liquid discharge $\omega = m\Omega$ nondimensionalized by the viscous time $\tau_\nu = (\nu/g^2)^{1/3}$.
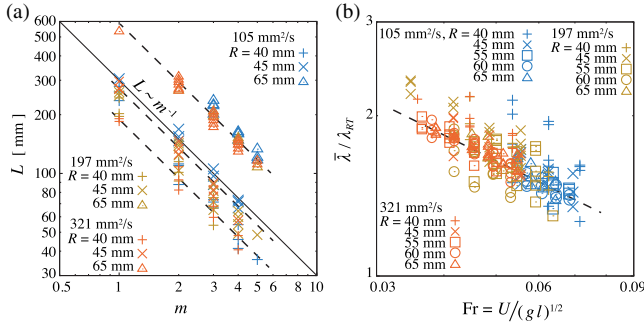
FIG. 5. Geometrical characteristics of spiral patterns. (a) The length L of each spiral arm. (b) The averaged wavelength $\bar{\lambda} = S/mL$ normalized by the wavelength of the fastest growing mode of the RT instability $\lambda_{RT}(= 2\pi\sqrt{2}l)$.

constant. The frequency ω is found to be scaled by the reciprocal of the viscous time $\tau_\nu = (\nu/g^2)^{1/3}$ [Fig. 4(a)], which characterizes the RT instability in a thick liquid layer [18]. The film radius R and the rate of liquid supply U have no significant effect on ω [Fig. 4(b)].

The most directly accessible spatial characteristic of a spiral pattern is the length of each arm, L. For a given set of values (R, U), this length is inversely proportional to the number of arms [Fig. 5(a)], implying that the total arm length mL of a pattern is constant. No influence of the fluid viscosity on L is detected. The total length mL is sensitive to the lateral extension of the film and proportional to the effective area of the film surface, $S = \pi(R^2 - R_0^2)$ [Fig. 5(a)]. It follows that the averaged wavelength, defined by $\bar{\lambda} = S/mL$, is constant at a given rate of liquid supply U. The wavelength $\bar{\lambda}$ decreases with U [Fig. 5(b)].

To reveal the mechanism of formation of spiral curtains one might invoke a phase diffusion equation with deriving characteristic functions involved from the first principles of fluid mechanics, as done for the spiral rolls in the Rayleigh-Bénard convection [7,21]. The application of the same method to the present problem is, nevertheless, challenging due to the unknown shape of free surfaces. In the studies of pattern formation in excitable media, theoretical modeling by cellular automata has allowed us to understand essential features of spiral patterns observed in experiments [4]. Insights into the formation of the spiral liquid curtains can also be obtained by constructing a cellular automaton (CA). In the present system, liquid discharged at a given location of the film is supplied either by the vertical flow through the grid plate or by the horizontal flow inside the film (Fig. 6). The flow rate of discharge J_0 per unit width of curtain is expressed as $J_0 = (V + c)b + U\delta$, where V is the horizontal liquid velocity toward the curtain averaged over the film thickness and c is the normal velocity of a liquid curtain. A length b represents the thickness of a film sublayer that is removed by the passage of a curtain, $b = U\Delta T$, where $\Delta T = 2\pi\omega^{-1} - \delta c^{-1}$ is the time interval between two successive passages of curtains. In the spiral
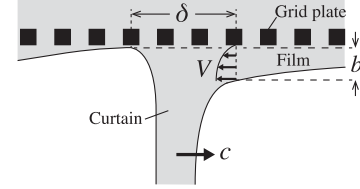

FIG. 6. Schematic drawing of a curtain cross section.

curtain regime, the horizontal liquid transport is negligible [22]. Thus, we have

$$J_0 \approx cb + U\delta = 2\pi Uc/\omega. \tag{1}$$

The negligible liquid transport inside the film may allow a simple CA. Regarding the film being constituted of cells uniformly distributed on the Cartesian grid, we model the dynamics of cells with the following rules. (1) Each cell is characterized by a thickness h representing the amount of liquid stored in the cell. It increases by a constant amount U per time step. (2) The cell discharges the stored liquid when h exceeds a critical value h_c, which is determined by the timescale of the RT instability, $h_c \sim U\tau_\nu$. (3) A discharging cell lowers the value of h_c locally to induce discharge of neighboring cells. This rule represents the capillary interaction between cells, which is necessary for the formation of liquid curtains. (4) The thickness of a discharging cell returns to zero at the next time step. Rotating spiral arms are indeed steady solutions of this CA, as shown in Fig. 7. Although these arms are initiated by a time-dependent forcing at the circular boundary, the spiral arms survive even after the forcing is turned off. The arms autoadjust their rotation speed and shape such that the phase of liquid discharge is locked for the arms to sweep every cell at a constant period dictated by the timescale of the RT instability.

An implicit hypothesis underlying the above CA model is a constant propagation speed of spiral arms, as the discharge advances by the linear dimension of a single cell per each time step. One can deduce the shape of a rotating arm, $r = F(\varphi - \Omega t)$, directly from the hypothesis, where (r, φ) are the cylindrical polar coordinates and the function
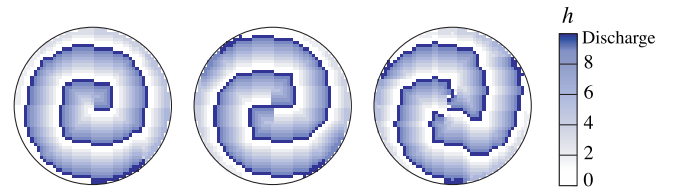

FIG. 7. Spiral arms generated by a CA model (see Appendix in Supplemental Material for details [16]). The arms are in steady counterclockwise rotation. The color scale indicates the local film thickness h in the unit of U. The critical thickness of discharge is set at $h_c = 9$. It is observed that the rotation speed of pattern Ω is inversely proportional to the number of spiral arms m, and that the period of discharge $1/m\Omega$ is identical to h_c.
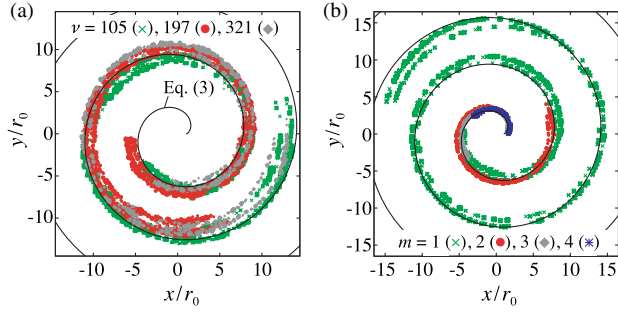
FIG. 8. The shapes of spiral arms. (a) In single armed patterns observed in different liquids of different viscosities ν ($R = 45$ mm, $U = 6.69$ mm/s). (b) In different patterns of different arm numbers m ($\nu = 321$ mm^2/s $R = 65$ mm, $U = 4.65$ mm/s). The length scale r_0 has been computed from measured wavelength $\bar{\lambda}$ [Eq. (4)]. The theoretical spiral shape [Eq. (3)] is shown in solid line for comparison.
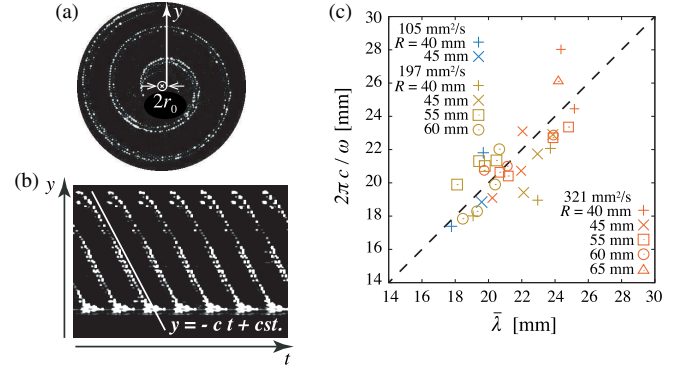

FIG. 9. The phase velocity c of a spiral arm. (a) A straight line perpendicular to a spiral arm. (b) A space-time diagram showing the invariance of the phase velocity c. (c) Comparison of the wavelength $\bar{\lambda}$ measured from the spiral length L and the wavelength $2\pi c/\omega$ estimated from c. Results are shown only for single armed spirals ($m = 1$).

F dictates the arm shape. Since the normal velocity c of an arm is given by a geometrical relationship [23],

$$c = \frac{\Omega F \partial_\varphi F}{\sqrt{F^2 + (\partial_\varphi F)^2}}, \tag{2}$$

the arm shape F is obtained by solving this differential equation. The solution is, in a parametric representation,

$$r = r_0 \sec\alpha, \qquad \varphi - \Omega t = \tan\alpha - \alpha + \varphi_0,$$

$$\left(0 < \alpha < \frac{\pi}{2}\right). \tag{3}$$

This solution involves only a single length scale $r_0 = c/\Omega$, which decides completely the shape of the arm.

The curve given by Eq. (3) is a spiral (Fig. 8). It recovers the Archimedean spiral far from the center, $r \gg r_0$. One can show that the length scale r_0 is related with the wavelength $\bar{\lambda}$:

$$2\pi r_0 = m\bar{\lambda}. \tag{4}$$

Since $\bar{\lambda}$ is constant at a given flow condition in the experiment, Eq. (4) implies that the shapes of arms in two patterns with different numbers of arms, say, m_1 and m_2, would be similar to each other with a scale factor m_1/m_2. Comparison with experiments shown in Fig. 8 supports the predicted shape [Eq. (3)] and the similarity law. For spiral arms given by Eq. (3), one can also show that any straight-line tangent to the circle $r = r_0$ is perpendicular to arms at any time instant t. The front of a spiral arm will thus advance at a constant speed c along the line. This behavior is confirmed for patterns of small arm numbers, $m = 1$ and 2 (Fig. 9). For larger m, the constant speed is limited within a small range of r due to geometrical confinement.

We have described a new example of rotating spiral patterns formed spontaneously in a fluid system. A simple CA model suggested that the motion of curtains synchronized with the RT instability would produce observed spiral patterns. The patterns have some distinctive features from spiral waves in reaction-diffusion systems. The latter waves give rise to outwardly rotating spirals in general, while the rotation direction may change if the system is close to the onset of Hopf bifurcation [24]. The phase velocity of the waves depends on the local curvature κ of a wave front and is dictated by the eikonal equation $c = c_\infty + D\kappa$, where c_∞ is the velocity of plane waves and D is the diffusion coefficient [25]. The spiral patterns considered in the present work, in contrast, rotate inwardly. Experimental observations suggest that the selection of rotation direction would be related to boundary effects rather than the distance from a bifurcation point. The phase velocity of spiral arms is independent of their local curvature, as suggested by Eq. (1) and supported by experimental results (Fig. 9). To some extent these differences may be explained from the nonoscillatory nature of the present medium and from the boundary effects generating liquid curtains. Theoretical investigations by model equations, e.g., the complex Ginzburg-Landau equation, which take into account these characteristics of the system, would be of interest to get further insight into the observed antispiral formation.

*Present address: Université Côte d'Azur, CNRS, Institut de Physique de Nice, 06100 Nice, France.
harunori@unice.fr

[1] M. Cross and H. Greenside, *Pattern Formation and Dynamics in Nonequilibrium Systems* (Cambridge University Press, New York, 2009).

[2] I. R. Epstein and K. Showalter, J. Phys. Chem. **100**, 13132 (1996).

[3] R. FitzHugh, Biophys. J. **1**, 445 (1961).

[4] M. Gerhardt, H. Schuster, and J. J. Tyson, Science **247**, 1563 (1990).

[5] E. Bodenschatz, J. R. de Bruyn, G. Ahlers,, and D. S. Cannell, Phys. Rev. Lett. **67**, 3078 (1991).

[6] B. B. Plapp, D. A. Egolf, E. Bodenschatz, and W. Pesch, Phys. Rev. Lett. **81**, 5334 (1998).

[7] M. Cross, Physica (Amsterdam) **97D**, 65 (1996).

[8] V. K. Vanag and I. R. Epstein, Science **294**, 835 (2000).

[9] Y. Gong and D. J. Christini, Phys. Rev. Lett. **90**, 088302 (2003).

[10] L. Limat, P. Jenffer, B. Dagens, E. Touron, M. Fermigier, and J. Wesfreid, Physica (Amsterdam) **61D**, 166 (1992).

[11] F. Giorgiutti, A. Bleton, L. Limat, and J. E. Wesfreid, Phys. Rev. Lett. **74**, 538 (1995).

[12] C. Counillon, L. Daudet, T. Podgorski, and L. Limat, Phys. Rev. Lett. **80**, 2117 (1998).

[13] C. Pirat, C. Mathis, P. Maïssa, and L. Gil, Phys. Rev. Lett. **92**, 104501 (2004).

[14] C. Pirat, A. Naso, J.-L. Meunier, P. Maïssa, and C. Mathis, Phys. Rev. Lett. **94**, 134502 (2005).

[15] C. Pirat, C. Mathis, M. Mishra, and P. Maïssa, Phys. Rev. Lett. **97**, 184501 (2006).

[16] See Supplemental Material at http://link.aps.org/supplemental/10.1103/PhysRevLett.122.014502 for rotating patterns observed in the experiment (Movies 1–4) and for the pattern generation process in the CA model (Movie 5). A detailed description of the CA model is also available (Appendix).

[17] P. Brunet, C. Clanet, and L. Limat, Phys. Fluids **16**, 2668 (2004).

[18] For a thin film attached to a horizontal solid plate and under no liquid supply, a linear stability theory based on the lubrication approximation predicts that the amplification of surface deformation due to the RT instability is characterized by a timescale $\tau_{\text{film}} = 12\gamma\nu/\rho g^2 b^3$, where b is the film thickness [19,20]. The fact that the frequency ω of liquid discharge is scaled by τ_ν^{-1}, but not by τ_{film}^{-1}, would arise from the boundary condition imposed by the grid plate: the flow velocity should match the vertical flow U at the plate. This condition is inconsistent with the lubrication theory, where the flow velocity is assumed horizontal. It would be satisfied better by a flow developing in a thick liquid layer, of which the velocity is rather vertical near the free surface. Further theoretical investigations should be performed for successful explanation of the scaling $\omega \sim \tau_\nu^{-1}$.

[19] M. Fermigier, L. Limat, J. E. Wesfreid, P. Boudinet, and C. Quilliet, J. Fluid Mech. **236**, 349 (1992).

[20] L. Limat, C. R. Acad. Sci. Paris, Sér. II **317**, 563 (1993).

[21] M. C. Cross and A. C. Newell, Physica (Amsterdam) **10D**, 299 (1984).

[22] According to experiments, $U \sim 1$ mm/s, $\delta \sim 5$ mm, $c \sim 10^2$ mm/s, $b \sim 2$ mm, and $V \sim 1$ mm/s.

[23] J. J. Tyson and J. P. Keener, Physica (Amsterdam) **32D**, 327 (1988).

[24] X. Shao, Y. Wu, J. Zhang, H. Wang, and Q. Ouyang, Phys. Rev. Lett. **100**, 198304 (2008).

[25] P. Foerster, S. C. Müller, and B. Hess, Proc. Natl. Acad. Sci. U.S.A. **86**, 6831 (1989).